Supporting Information

Biomimetic Nanoparticles Directly Remodel Immunosuppressive Microenvironment for Boosting Glioblastoma Immunotherapy

Tingting Wang [a], Hao Zhang [a], Weibao Qiu [b], Yaobao Han[a], Hanghang Liu[a], Zhen Li[a]*

[a]Center for Molecular Imaging and Nuclear Medicine, State Key Laboratory of Radiation Medicine and Protection, School for Radiological and Interdisciplinary Sciences (RAD-X), Soochow University, Collaborative Innovation Center of Radiation Medicine of Jiangsu Higher Education Institutions
Suzhou 215123, P. R. China
Email: zhenli@suda.edu.cn

[b]Paul C. Lauterbur Research Center for Biomedical Imaging, Institute of Biomedical and Health Engineering, Shenzhen Institutes of Advanced Technology, Chinese Academy of Sciences,
Shenzhen 518055, P. R. China

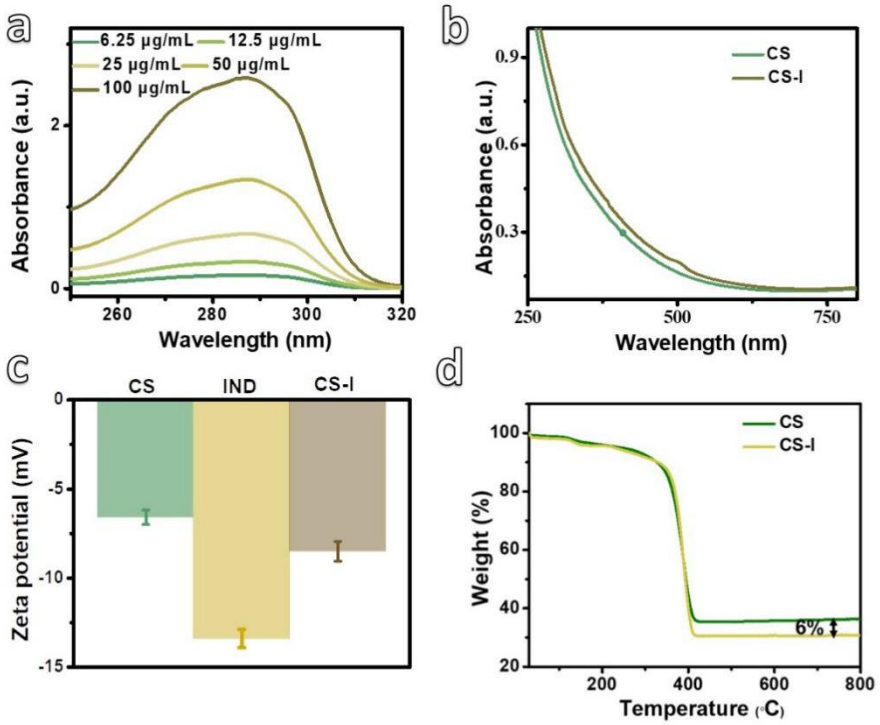

Fig. S1. (**a**) UV-*vis*-NIR absorbance of different concentrations of IND in H_2O. (**b**) UV-*vis*-NIR absorbance of CS and CS-I NP solutions with the same concentration. (**c**) Zeta potentials of CS NPs, IND and CS-I NPs. (**d**) TGA curves of cyclodextrin modified $Cu_{2-x}Se$ nanoparticles (CS NPs) and CS-IND nanoparticles (CS-I NPs).

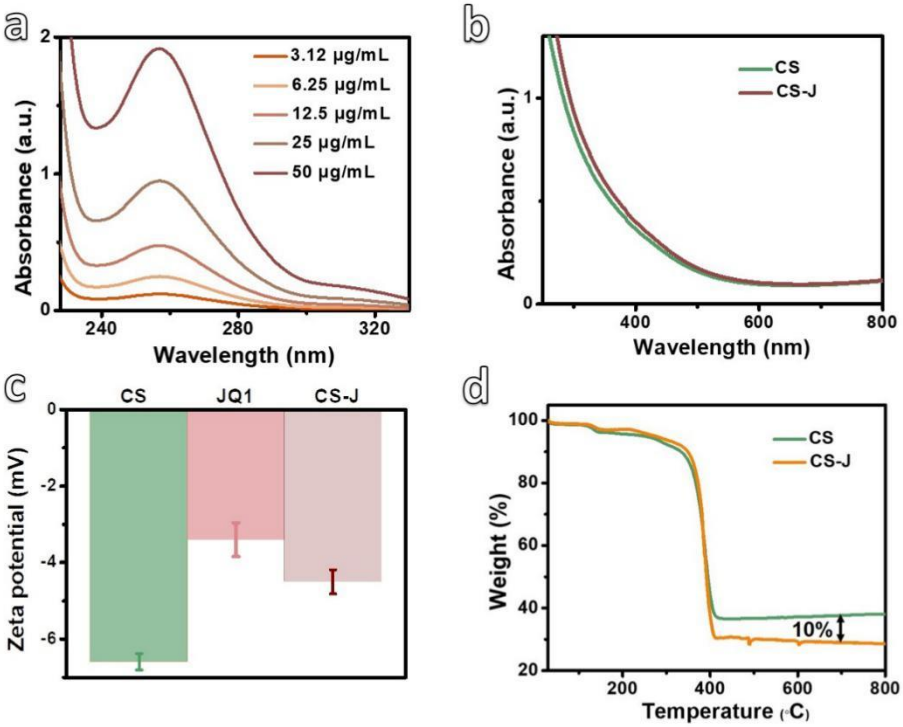

Fig. S2. (**a**) UV-*vis*-NIR absorbance of different concentrations of JQ1 in H_2O. (**b**) UV-*vis*-NIR absorbance of CS and CS-J NP solutions with the same concentration. (**c**) Zeta potentials of CS NPs, JQ1 and CS-J NPs. (**d**) TGA curves of cyclodextrin modified $Cu_{2-x}Se$ nanoparticles (CS NPs) and CS-JQ1nanoparticles (CS-J NPs).

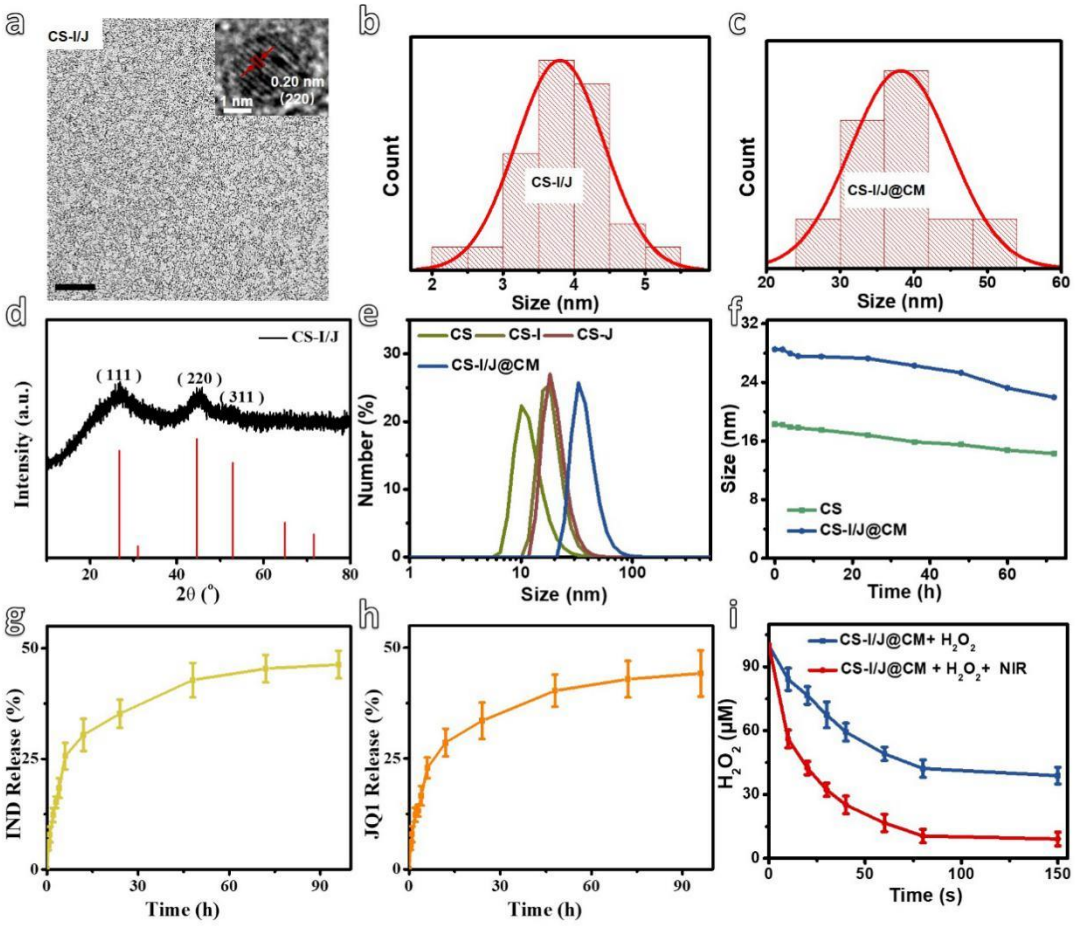

Fig. S3. (**a**) TEM image of ultrasmall CS-I/J NPs (scale bar: 50 nm) with an inset of high-resolution TEM image. (**b-c**) Histograms of the particle size distribution of CS-I/J NPs and CS-I/J@CM NPs. (**d**) XRD pattern of ultrasmall CS-I/J NPs in comparison with standard peaks of cubic berzelianite (JCPDS Card No. 06-0680). (**e**) Hydrodynamic sizes of CS, CS-I, CS-J, and CS-I/J@CM NPs. (**f**) Hydrodynamic size of CS or CS-I/J@CM NPs dispersed in PBS solutions for different time. (**g**) Release profiles of IND from CS-I@CM NPs in PBS. (**h**) Release profiles of JQ1 from CS-J@CM NPs in PBS. (**i**) Degradation of H_2O_2 (400 μM) catalyzed by CS-I/J@CM NPs (12.5 μg/mL) and irradiated with or without 1064 nm laser (0.75 W/cm^2, 5 min, n=3).

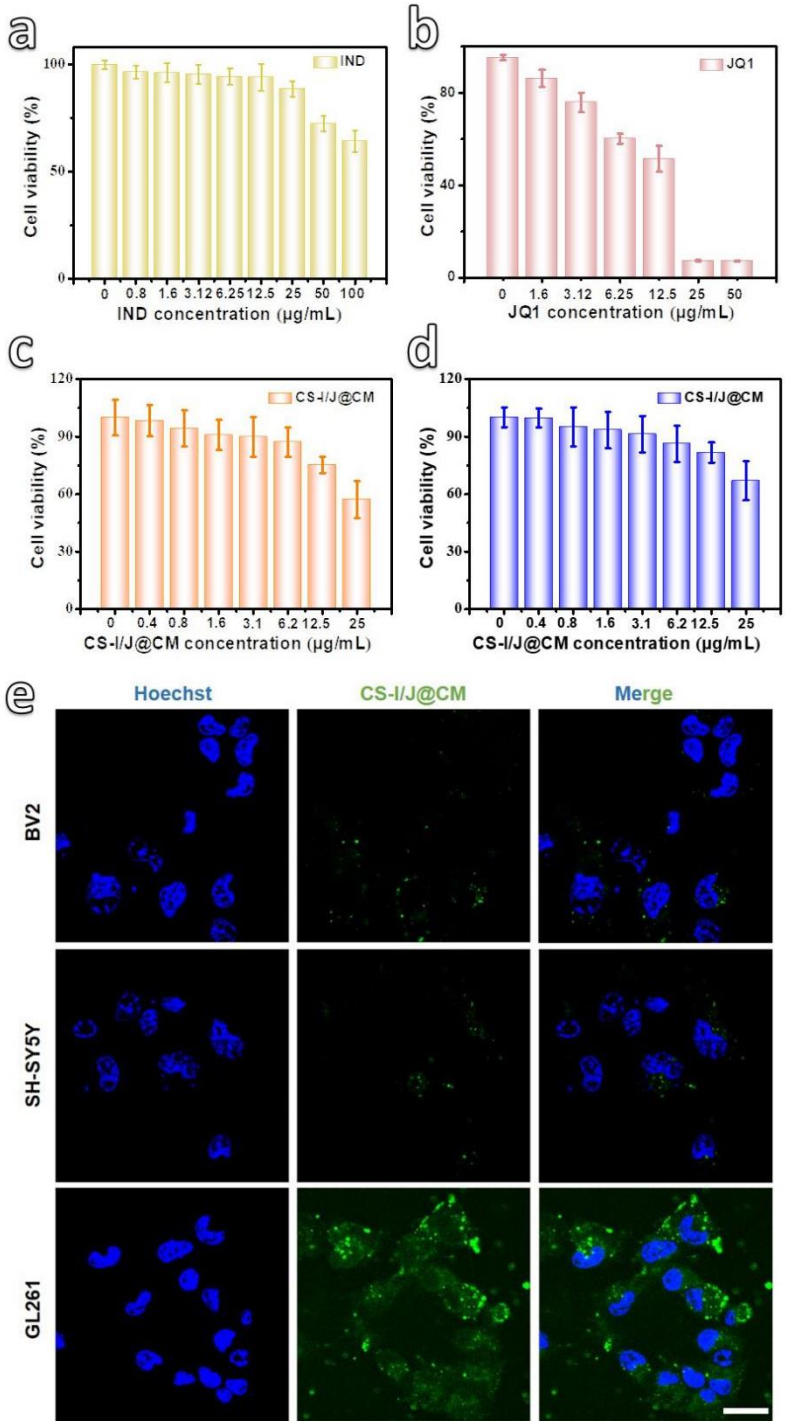

Fig. S4. Viability of GL261 cells cultured with different concentrations of (**a**) IND and (**b**) JQ1. (**c**) Viability of SH-SY5Y cells cultured with different concentrations of CS-I/J@CM NPs.(**d**) Viability of BV2 cells cultured with different concentrations of CS-I/J@CM NPs. (**e**) CLSM images of BV2 cells, SH-SY5Y cells, and GL261 cells, respectively, cultured with CS-I/J@CM NPs for 4 h to show the homologous adhesion of nanoparticles (GL261 CMs were labeled with DiO (green FL)). The nuclei were stained blue with Hoechst 33342 (scale bar: 20 μm).

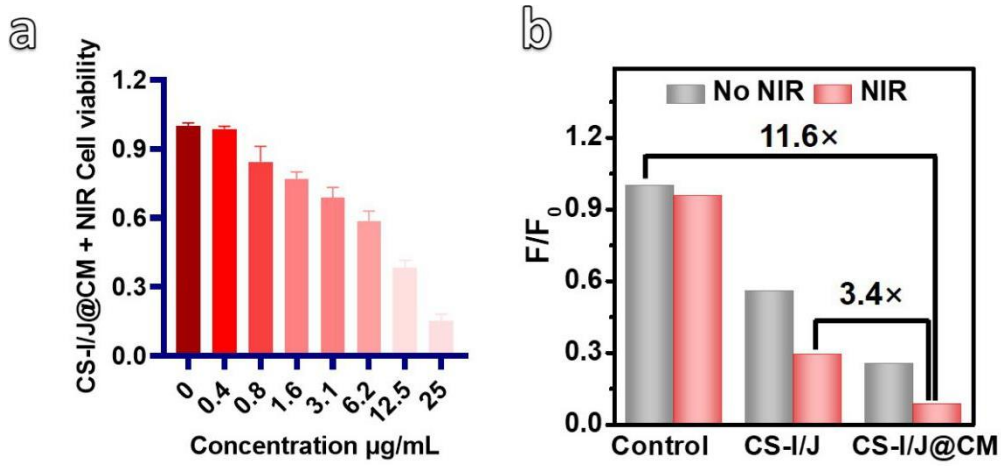

Fig. S5. (**a**) Viability of G261 cells cultured with different concentrations of CS-I/J@CM NPs under irradiation. (**b**) Quantification of hypoxia degree of MCTSs through CLSM.

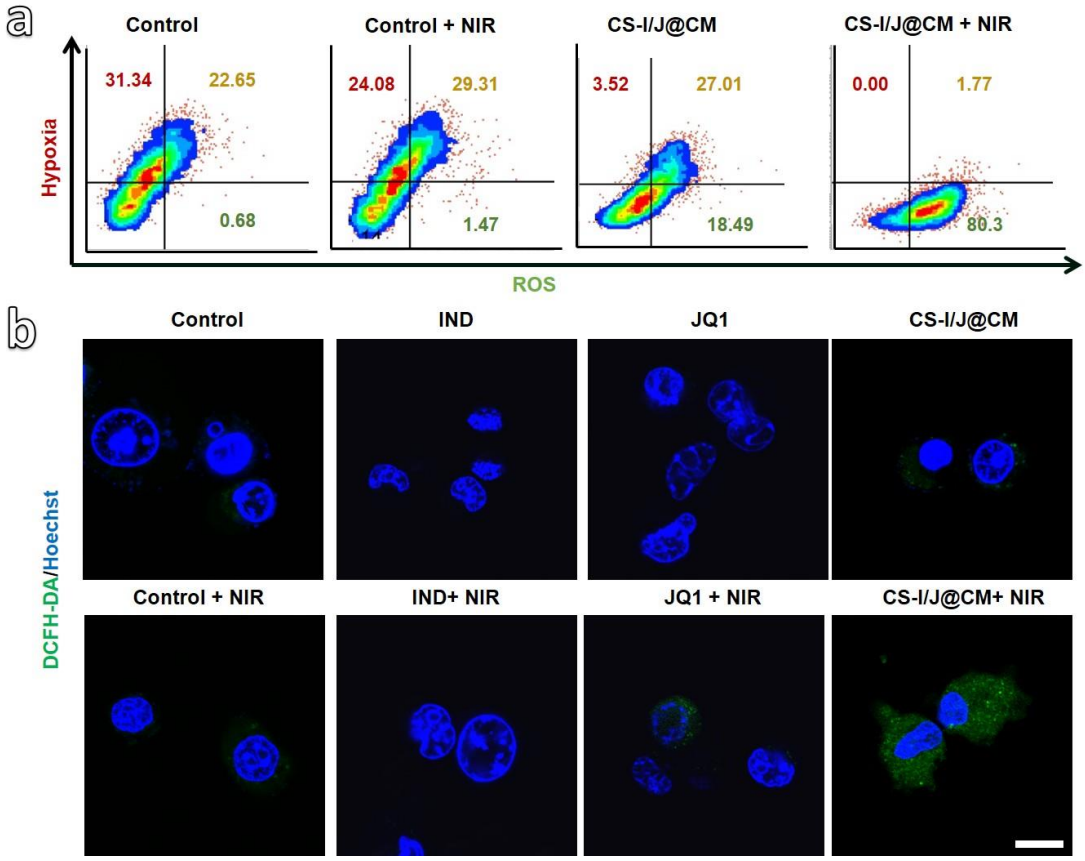

Fig. S6. (**a**) The flow cytometry analysis of hypoxia and ROS in GL261 cells cultured under different conditions. (**b**) The CLSM of ROS produced in GL261 cells cultured under different conditions (scale bar: 10 μm).

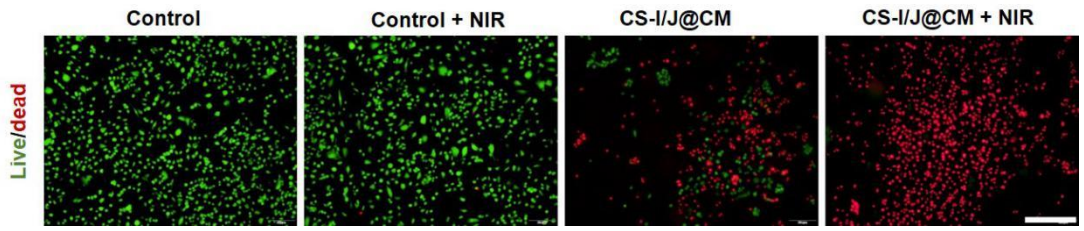

Fig. S7. Fluorescence images of GL261 cells stained with a live/dead kit after irradiation with or without a 1064 nm laser (scale bar: 200 μm).

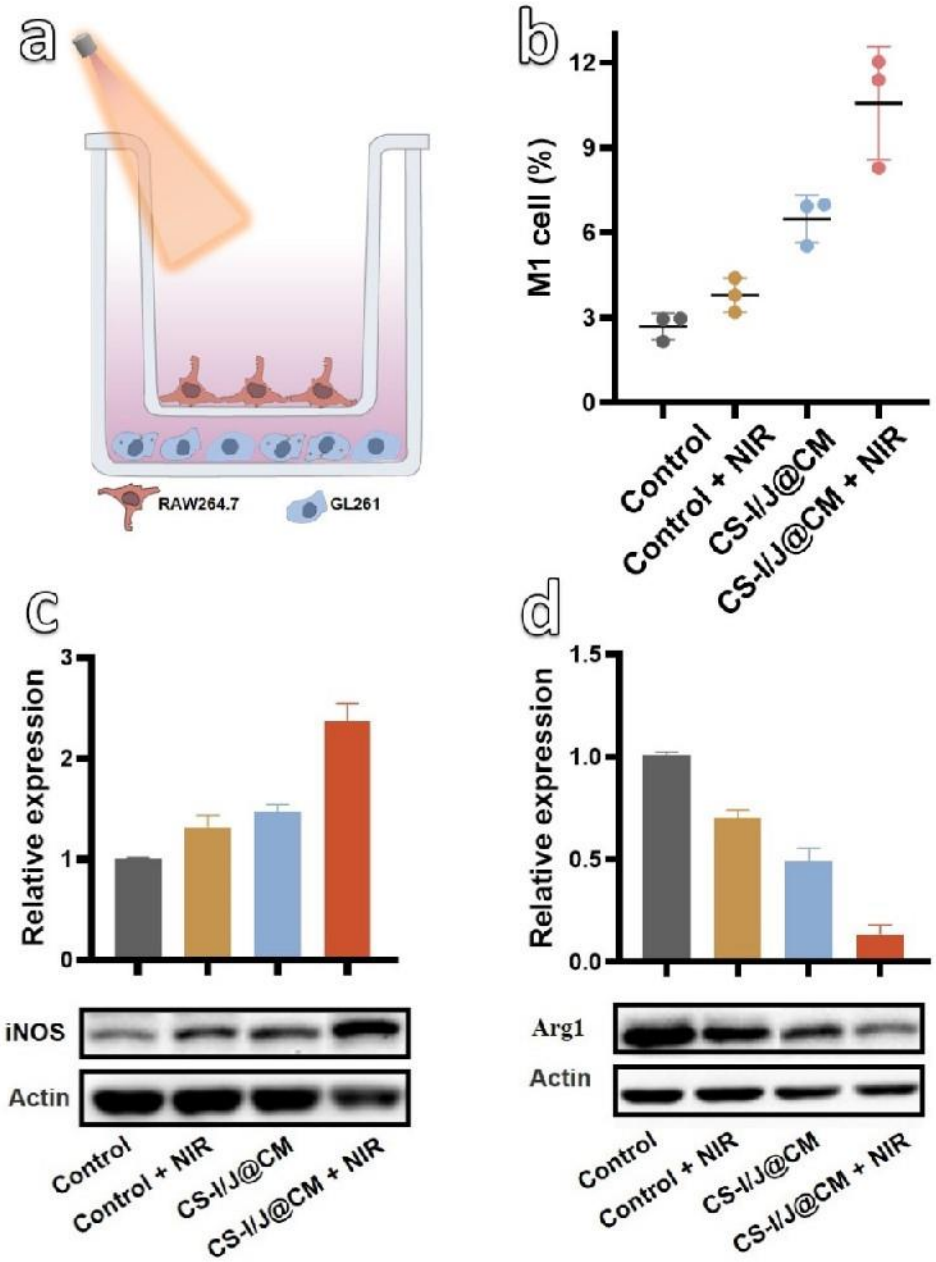

Fig. S8. (**a**) The schematic illustration of co-culturing RAW 264.7 and GL261 cells in a transwell setup. (**b**) Flow cytometry analysis of M1 macrophages after different treatments. Detection Western-blot of (**c**) iNOS and (**d**) Arg1 expressions in the GL261 cells after different treatments.

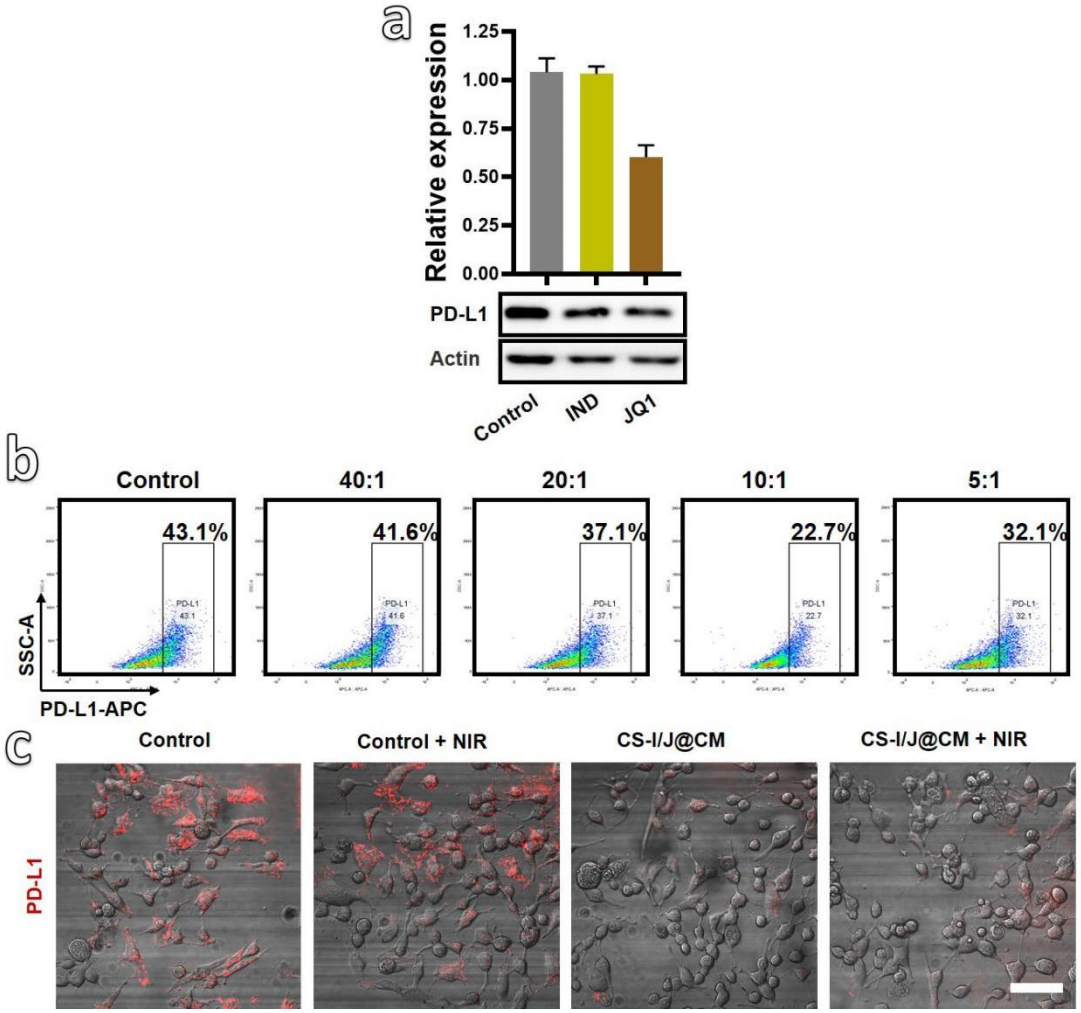

Fig. S9. (**a**) Detection of PD-L1 expression in the GL261 cells of different groups by Western-blot. (**b**) Flow cytometry analysis of PD-L1 expression on GL261 cells after treatments with different ratios of CS-I NPs and CS-J NPs. (**c**) The CLSM of PD-L1 expressed by GL261 cells after different treatments (scale bar: 50 μm).

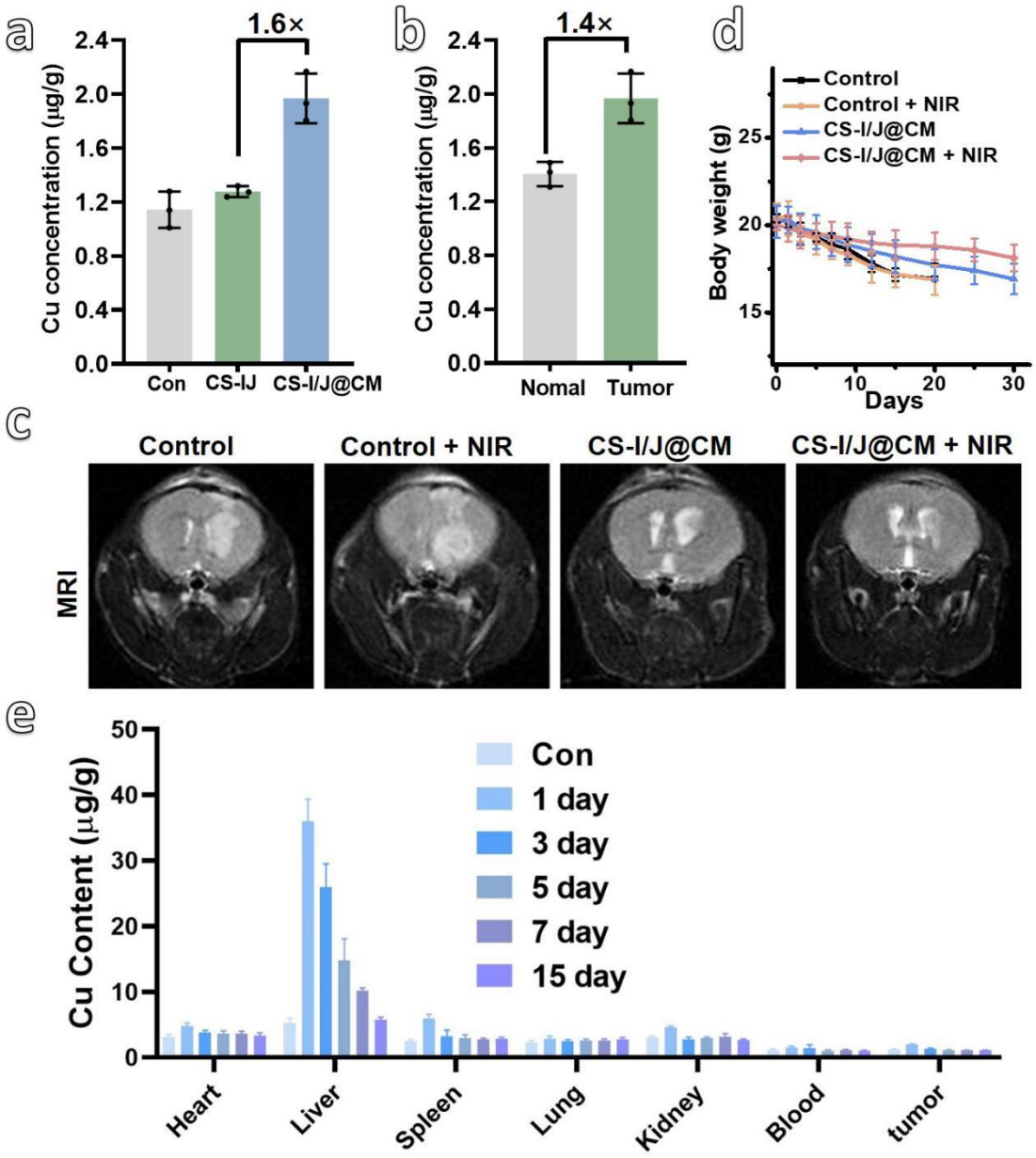

Fig. S10. The copper concentration in tumors measured by ICP-MS after 8 h intravenous injection of (**a**) CS-I/J NPs or CS-I/J@CM NPs into mice bearing GBM tumors. (b) CS-I/J@CM in normal brain of healthy mice, or in tumors of glioma mice. (c) Magnetic resonance imaging (MRI) of brain of mice bearing GBM tumors after different treatments for 13 d. (d) Weights of mice after different treatments. (**e**) The biodistribution of CS-I/J@CM NPs after intravenous injection into glioblastoma -bearing mice, as determined by measuring Cu concentrations in tissue lysates with ICP-MS.

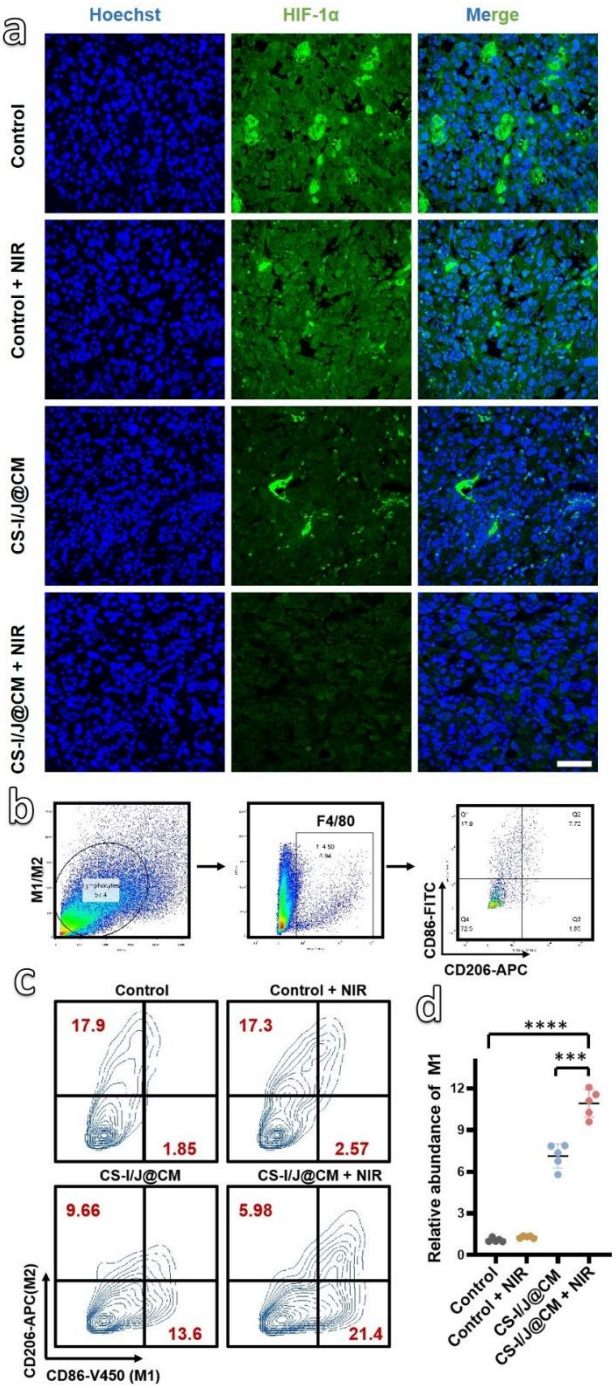

Fig. S11. (**a**) Images of stained tumor sections for detection of hypoxia-inducible factor-1 (HIF-1*α*) from different groups of mice sacrificed after 1 day treatment (scale bar: 40 μm). (**b-c**) Flow cytometry gating strategy and analysis for M1 macrophages ($F4/80^+CD86^+$) and M2 ($F4/80^+CD206^+$) in tumor tissue. (**d**) Normalization of the M1 macrophages in (**c**). (*p < 0.05, **p < 0.01, ***p < 0.001, ****p<0.0001, n = 5)

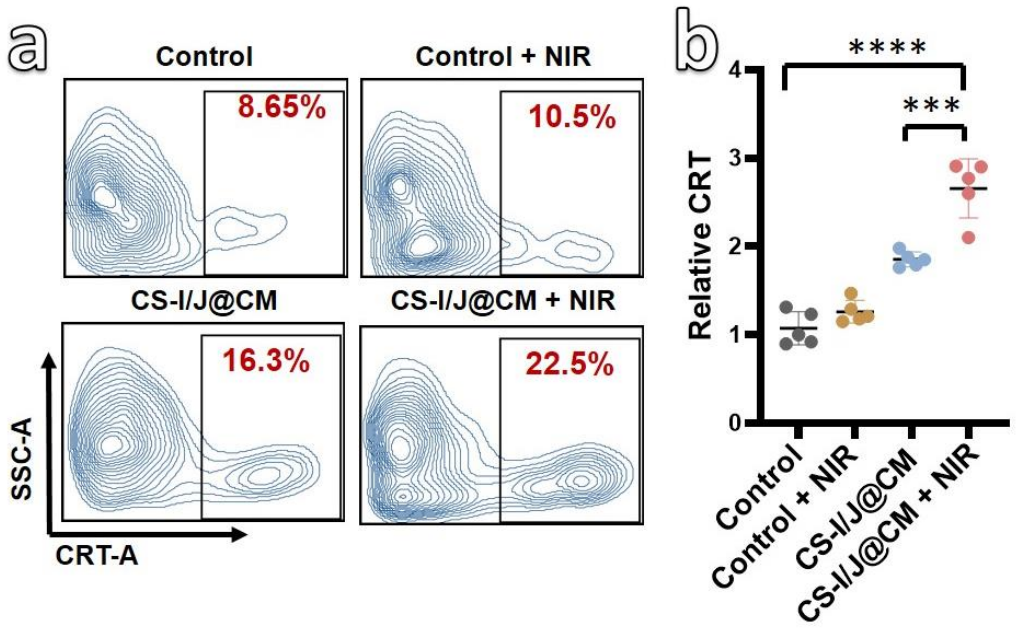

Fig. S12. Flow cytometry analysis of CRT exposure in tumors of mice after different treatments and the normalization. (*p < 0.05, **p < 0.01, ***p < 0.001, ****p<0.0001, n = 5)

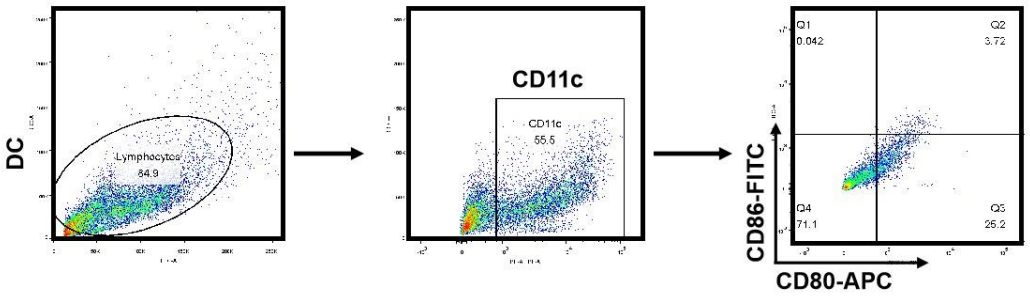

Fig. S13. Flow cytometry gating strategy for Fig. 5f.

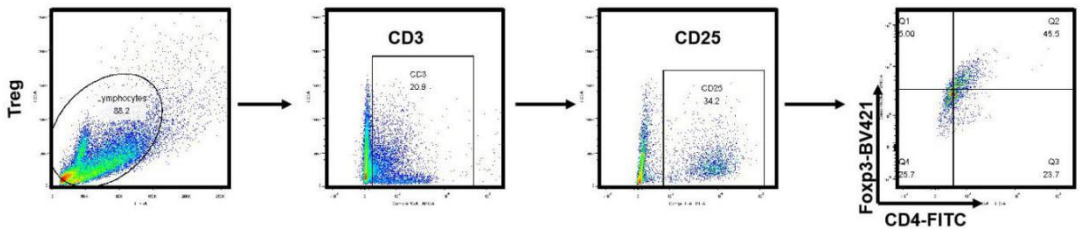

Fig. S14. Flow cytometry gating strategy for Fig. 6e.

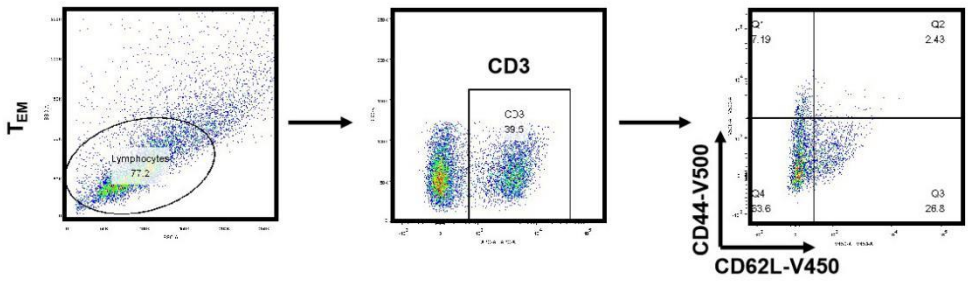

Fig. S15. Flow cytometry gating strategy for Fig. 6g.

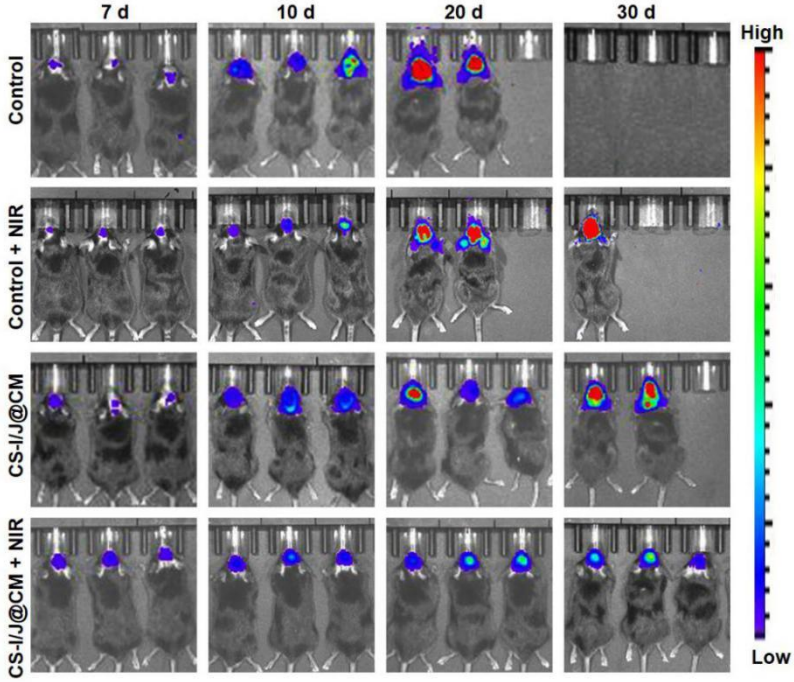

Fig. S16. Bioluminescence images of mice from different treatment groups.

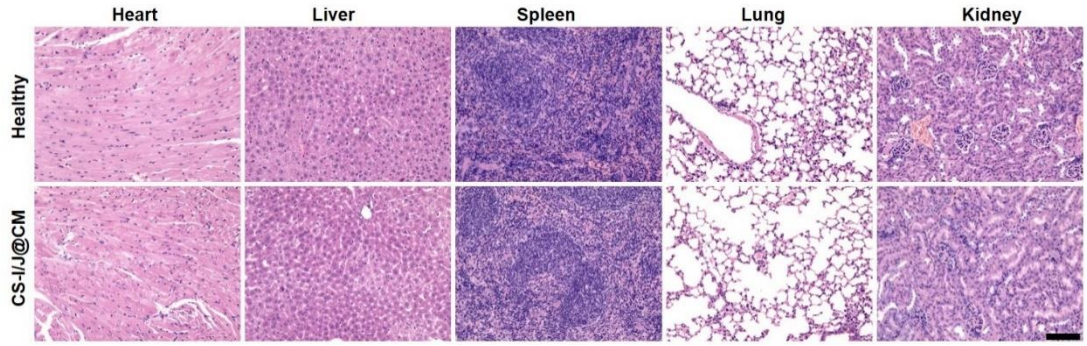

Fig. S17. H&E staining of major organs (heart, liver, spleen, lung and kidney) collected from GL261 tumor-bearing mice at 7 days after intravenous injection of CS-I/J@CM NPs, in comparison with those of healthy mice. There is no obvious damage to these tissues. (Scale bar: 100 μm)